Experimental verification of the Kruskal-Shafranov stability limit in line-tied partial-toroidal plasmas

E. Oz,[a] C. E. Myers, M. Yamada,[b] H. Ji, R. M. Kulsrud, and J. Xie[c]
Princeton Plasma Physics Laboratory, Princeton, New Jersey 08543, USA

(Received 17 June 2011; accepted 15 September 2011; published online 19 October 2011)

The stability properties of partial-toroidal flux ropes are studied in detail in the laboratory, motivated by ubiquitous arched magnetic structures found on the solar surface. The flux ropes studied here are magnetized arc discharges formed between two electrodes in the Magnetic Reconnection Experiment (MRX) [Yamada *et al.*, Phys. Plasmas **4**, 1936 (1997)]. The three dimensional evolution of these flux ropes is monitored by a fast visible light framing camera, while their magnetic structure is measured by a variety of internal magnetic probes. The flux ropes are consistently observed to undergo large-scale oscillations as a result of an external kink instability. Using detailed scans of the plasma current, the guide field strength, and the length of the flux rope, we show that the threshold for kink stability is governed by the Kruskal-Shafranov limit for a flux rope that is held fixed at both ends (i.e., $q_a = 1$). © *2011 American Institute of Physics*. [doi:10.1063/1.3647567]

I. INTRODUCTION

Coronal mass ejections[1] (CMEs), which are the most energetic events in the solar system, have been linked to a variety of heliospheric structures including eruptive prominences,[2,3] interplanetary magnetic clouds,[4] and plasmoids ejected from coronal arcades.[5,6] One model that is commonly invoked to describe the magnetic topology of these structures is the twisted flux rope.[3,7–10] This magnetic configuration is potentially unstable to the current-driven external kink instability, which has long been suggested as a possible mechanism for solar eruptions.[11] Ongoing observational,[12] theoretical,[13] and numerical[14–16] analysis suggests that the kink instability can cause coronal magnetic flux ropes to erupt, though others have concluded that these flux ropes should be kink-stable due to equilibrium expansion.[17] Despite rapid progress in observational capabilities, the lack of detailed magnetic measurements in crucial areas of the corona has prevented the conclusive study of kink stability in flux-rope-like coronal magnetic structures. In contrast to remote-sensing observations, laboratory experiments offer *in situ* measurements that can contribute to the understanding of solar-relevant plasma phenomena such as kink stability.

The kink stability of a cylindrical magnetic flux rope is often quantified in terms of the so-called "safety factor," q, which is given by

$$q(r) = \frac{2\pi}{L}\frac{rB_T}{B_P(r)}, \tag{1}$$

where r is the radial distance from the flux rope axis, B_T is the externally-applied "toroidal" magnetic field, B_P is the plasma-produced "poloidal" magnetic field, and L is the length of the flux rope. The safety factor measures the pitch of the field lines as they helically wind around the axis of the flux rope. If the field line pitch becomes too steep (i.e., q becomes too low), the flux rope will kink in response to long-wavelength magnetic perturbations. The onset of the most dangerous kink mode, the external kink, depends only on the value of the "edge" safety factor q_a:

$$q_a \equiv q(a) = \frac{(2\pi a)^2 B_T}{\mu_0 I_p L}, \tag{2}$$

where a is the minor radius of the flux rope and I_p is the total plasma current. As first derived by Kruskal and Shafranov, a flux rope will become unstable to the external kink mode when q_a drops below the $q_a = 1$ threshold.[18,19] This so-called Kruskal-Shafranov (KS) limit, which was derived assuming periodic flux rope boundary conditions, has been quite successful in explaining the stability of periodic (toroidal) laboratory plasmas such as tokamaks.[20] The analysis becomes more complicated, however, when considering non-periodic flux ropes such as those found in the solar corona.

Non-periodic flux ropes can be produced in the laboratory using magnetized discharges formed between two electrodes. The stability characteristics of such plasmas are predicted to be inherently dependent on the boundary conditions at the two flux rope footpoints. A given footpoint can either be "fixed" (where displacements vanish) or "free" (where stresses vanish). In the case where both footpoints are fixed, the flux rope is predicted to obey the standard $q_a = 1$ KS limit.[21,22] If, on the other hand, only one end of the flux rope is fixed and the other is free, the stability limit is predicted to change to $q_a = 2$.[23]

The two flux rope boundary configurations introduced above (dual-fixed and fixed/free) are of keen experimental interest. At the cathode end of the discharge, the magnetic field lines are frozen into both the conducting cathode

[a]Electronic mail: eoz@usc.edu.
[b]Electronic mail: myamada@pppl.gov.
[c]Permanent address: CAS Key Laboratory of Plasma Physics, Department of Modern Physics, University of Science and Technology of China, Hefei 230026, China.

material and the nearby plasma. This so-called "line-tying" effect ensures that at least the cathode end of the flux rope is a fixed boundary. The boundary condition at the anode, however, is much more complicated. Electrons in the plasma near the anode are not as mobile as those near the cathode, so tangential electric fields can arise in the anode sheath region. These tangential electric fields break the ideal magnetohydrodynamic (MHD) line-tying condition and permit the flux rope to slide around on the anode surface.[23] The actual anode boundary condition (fixed or free) is therefore set by some mechanism other than line-tying such as the geometry of the anode itself. This complexity at the anode boundary has so far prevented a definitive experimental study of kink stability in dual-fixed-boundary flux ropes.

Experiments conducted in a linear device have demonstrated a range of anode boundary conditions. First, a free boundary condition was observed in discharges where a thin flux rope is terminated by a large anode plate.[24] In these experiments, the criterion for the onset of the external kink mode was found to be $q_a = 2$, indicating that the flux rope exhibits fixed/free stability behavior. In an attempt to force the anode to instead act as a fixed boundary, several different conical electrodes were used to inhibit the movement of the flux rope's free end.[25] Six anodes with increasingly restrictive conical shapes were shown to confine the motion of the flux rope and increase its stability against the kink mode. While stability thresholds in the range of $2 \geq q_a \gtrsim 1.2$ were observed using this technique, full $q_a = 1$ fixed-boundary behavior was not achieved.

Experiments with open-ended plasma plumes have correlated the $q_a = 1$ KS limit to the onset of kink stability.[26,27] In these devices, the plasma does not interact directly with the anode; instead, it terminates at a plasma/vacuum interface as it streams away from the cathode. Though the line-tied (fixed) condition at the cathode is expected, it is not obvious that the plasma/vacuum interface should act as a second fixed boundary. Both experimental groups cite the Alfvénic discontinuity that results from a strong density gradient at the plasma/vacuum interface as a possible cause of the observed stability behavior. Because of the uncertainty surrounding this boundary condition at the open end, however, these experiments do not constitute a definitive study of kink stability in dual-fixed-boundary systems.

A third experimental study was carried out with a linear screw pinch plasma where clear evidence of a kink mode was observed.[28] Here, the mode onset is attributed to q dropping below unity in the interior of the plasma. Consequently, the authors conclude that the plasma exhibits dual-fixed-boundary stability behavior. It is interesting to note, however, that the edge q value crosses the $q_a = 2$ threshold at nearly the same time that q drops below unity inside the plasma. It is therefore conceivable that the discharge instead has a fixed/free boundary configuration. In this scenario, the external kink would trigger from $q_a = 2$ at the edge rather than from $q < 1$ internally. Thus, despite the existing body of work summarized here, we conclude that the predicted $q_a = 1$ threshold for dual-fixed-boundary kink stability has not been conclusively demonstrated in the laboratory.

In this paper, we present definitive evidence that magnetic flux ropes formed between two equally-sized electrodes do, in fact, exhibit the $q_a = 1$ KS threshold for dual-fixed-boundary stability. We quantitatively support this conclusion with stability measurements from detailed scans of the plasma current, toroidal field strength, and flux rope length. The restricted motion of the flux rope at the anode footpoint, which is required in order to have a second fixed boundary, is attributed to the direct matching between the minor radius of the anode plate and the minor radius of the flux rope (as set by the cathode). Additionally, the flux ropes studied here have a partial-toroidal geometry and are therefore potentially relevant to structures found in the solar corona. Several experimental groups have previously studied partial-toroidal plasmas in the laboratory,[29–31] but the stability properties of these plasmas have not been not quantitatively investigated.

II. EXPERIMENTAL SETUP

The experiments reported here were conducted in the Magnetic Reconnection Experiment (MRX) facility.[32] In order to form a partial-toroidal flux rope, an arc discharge is created between two electrodes of equal size that are separated by a toroidal angle Θ that can be varied between 90° and 270° (see Figs. 1 and 2). The electrodes are each copper disks of minor radius $a = 7.3$ cm that are centered at a major radius of $R = R_0 = 19.5$ cm (Fig. 2(b)). The stainless steel wall of the vacuum vessel is located far away from the electrodes at $R = 76.2$ cm. The electrodes are powered by a capacitor bank with typical voltages of 3–10 kV and up to 50 kJ of stored energy. The electrode circuit is constructed with a double feed-through in order to minimize its inductance. Large circular coils outside the ends of the vacuum vessel provide a z-directed strapping (equilibrium) field, B_E, of up to 200 G that is largely uniform in time and space. A separate set of eight three-turn coils thread the center of the device and produce a toroidal (θ-directed) guide field, B_T. This guide field coil set, which is powered by a stand-alone 0.5 F, 450 V capacitor bank, provides up to 1500 G of toroidal field at the center of the copper electrodes.

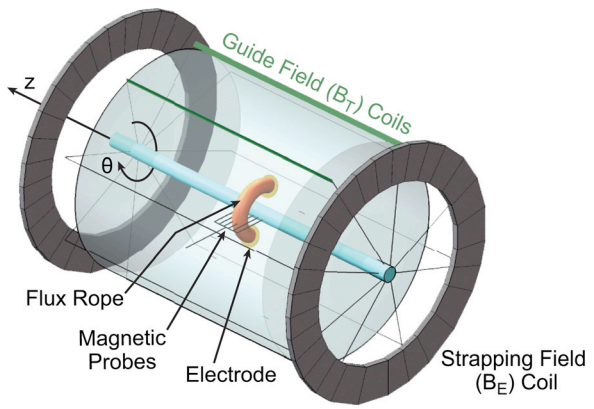

FIG. 1. (Color online) A schematic of the experimental setup. A plasma arc (flux rope, orange) with major radius $R_0 = 19.5$ cm is maintained between two electrodes. Current through the center column (center blue and return paths green) provides the toroidal guide field, B_T, along the plasma arc; a pair of external coils (big gray circles) provides the equilibrium field (B_E) along the Z direction. The plasma current provides the poloidal field that twists the field lines in the flux rope. Also shown is the 2D 90-channel magnetic probe array.

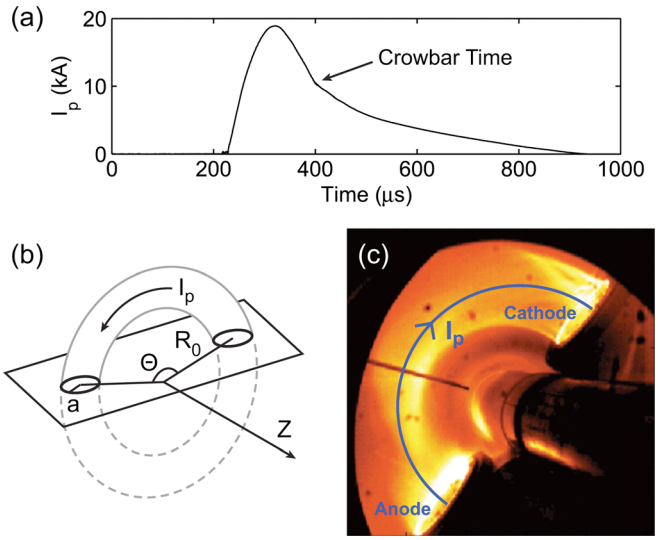

FIG. 2. (Color online) (a) A typical plasma current waveform $I_p(t)$. (b) A schematic of the current loop with minor radius a, electrode major radius R_0, and electrode separation angle Θ. (c) A visible light image of a flux rope plasma taken by a fast framing camera with 1 μs exposure.

The working gas is puffed in before the plasma is formed and fills the vacuum vessel to a uniform pressure of several mTorr. The gas puff is controlled by piezoelectric valves that inject gas at the machine wall or through small holes in the electrodes. This configuration permits the use of a mixture of gases to achieve ionization at lower applied voltages. Experiments conducted with various gas species such as H, D, He, Ar and pressure scans from 1–100 mTorr showed few discernable changes in the flux rope dynamics. All of the experimental data that is shown in Secs. III and IV are taken from hydrogen shots where the gas was injected only at the machine wall. The fill pressures for these discharges ranged from 10–20 mTorr.

A typical flux rope discharge in MRX lasts for $t_D \sim 700$ μs, which is much longer than the $t_A \sim 1.0$ μs Alfvén transit time. Other partial-toroidal flux rope experiments are significantly more transient with $t_D \sim 10$ μs and $t_A \sim 0.5$ μs.[29,30] A sample flux rope plasma current waveform $I_p(t)$ is shown in Fig. 2(a). The shape of this waveform is determined by the characteristics of the driving circuit, which includes the capacitor bank, its connections to the electrodes, and the plasma arc itself. High power diodes are included in the forward part of the driving circuit such that when the "crowbar" circuit is closed at $t \simeq 400$ μs, the plasma current waveform decays monotonically thereafter as a simple L-R circuit. This monotonic decay is crucial for clearly identifying the kink stability threshold. An oscillating waveform, on the other hand, would drive the flux rope back and forth across the stability threshold, thereby significantly complicating the stability analysis.

The MRX flux rope plasmas are monitored with a variety of magnetic probes, including a rake-shaped 90-channel probe array that measures all three components of the magnetic field at 30 locations in a 2D (Z-R) plane. Each individual magnetic field measurement is the integral of the voltage induced by the plasma's changing magnetic field on a particular $\dot{B}$ pickup coil within the probe. Collectively, these measurements permit the reconstruction of the current density profile $J_T(Z,R)$ within the flux rope at one toroidal location. Several additional magnetic probes are included at various other toroidal locations along the flux rope. These additional probes are 1D (radial) probes that measure the axial field profile $B_Z(R)$ along their length. The radial location where each $B_Z(R)$ profile reverses sign corresponds to the location of the magnetic axis of the flux rope at that toroidal location. By combining these measurements, the R-θ profile of the flux rope can be reconstructed as a function of time. This profile provides a measurement of the length of the flux rope $L(t)$ that is used in the stability analysis. The signals from each of these magnetic probes are digitized at 2.5 MHz (every 0.4 μs), which is slightly faster than the Alfvén transit time ($t_A \sim 1.0$ μs). Additionally, a fast charge-coupled device (CCD) camera is used for monitoring the 3D dynamic evolution of each discharge in the visible spectrum. Frames can be captured every 4–12 μs with a 1 μs exposure time.

III. FEATURES OF THE FLUX ROPE PLASMAS

The partial-toroidal flux ropes produced in MRX expand radially as a result of "hoop" forces from the arched plasma current channel. This expansion is countered by the inward force from the strapping field B_E and by tension in the entrained toroidal field B_T. Thus, because the flux ropes are driven on timescales that are much longer than the Alfvén time, they evolve through a series of equilibria where the various radial forces are in balance. Such force balance does not, however, guarantee stability. Under certain conditions, the flux ropes are observed to undergo kink oscillations about the aforementioned partial-toroidal equilibrium.

Figure 3 shows measurements from two sample discharges with different stability properties. The upper row of panels for each discharge shows visible light snapshots taken at four different times by the fast framing camera (false color is added later). The lower row of panels shows the measured poloidal magnetic field vectors and the corresponding current density as measured by the rake-shaped 90-channel magnetic probe. When substantial toroidal field is applied, the flux rope remains stable and does not move around (Fig. 3(a)). If the toroidal field strength is reduced, however, then the flux rope kinks wildly (Fig. 3(b)). Note that the visible light amplitude correlates well with the current density. The first visible light image in the unstable case reveals some of the helical structure of the kink instability as it can be seen twisting from the cathode to the anode.

Fast framing camera movies that track the complete evolution of the flux rope show that kink unstable flux ropes in MRX make rigid body rotations. These rotations can also be seen in the magnetic data. In particular, measurements from the 2D 90-channel magnetic probe can be used to track the rotation of the Z-R flux rope center at one toroidal location. For this analysis, the flux rope center is defined as the center-of-mass of the 2D current density profile as measured by the magnetic probe. Because the integrated plasma current measured by the probe is within 10% of the total plasma current, the center-of-mass of the current density profile is a meaningful measurement of the flux rope center. The time evolution of the Z-R flux rope center during

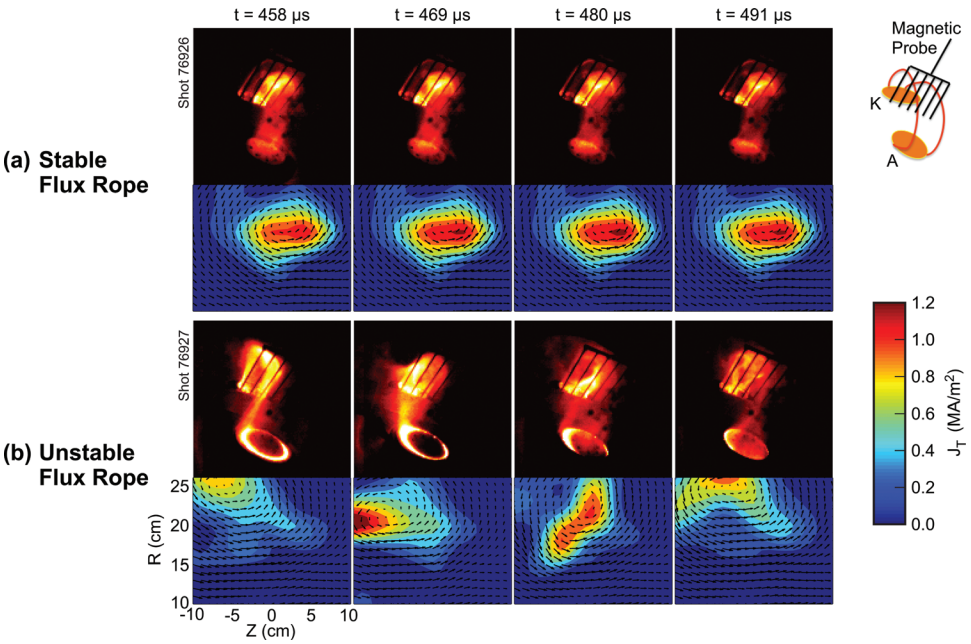

FIG. 3. (Color) Measurements from two flux ropes with different applied toroidal fields. For each flux rope, false color visible light images and magnetic measurements are shown for four different times. The diagram at the top right illustrates the electrode setup as seen by the fast framing camera. The corresponding contour plots show the measured poloidal magnetic field vectors and the resulting toroidal current density J_T. The stable flux rope (a) has sufficient toroidal field to avoid kinking, while the unstable flux rope (b) has lower toroidal field and kinks throughout the progression.

a sample discharge is shown in Fig. 4. False color is added for better visualization. The plasma column rotates steadily during the high current phase of the discharge before stabilizing later in time.

The rigid body rotations shown in Fig. 4 vary in frequency between 30–90 kHz. We are able to correlate this behavior to the external kink instability using reconstructions of the flux rope profile that are derived from the toroidally-distributed 1D magnetic probes. The measured flux rope profile (not shown here) is $n=1$ in character and rotates coherently in time. Thus, the rigid body rotation shown in Fig. 4 is simply the manifestation of the coherently-rotating kink mode at a single toroidal location. The rotation of the kink mode is likely driven by plasma flowing toroidally from cathode to anode. Ryutov *et al.* showed that flows of this type will drive the mode to rotate with its helical profile screwing out of the cathode and into the anode.[23] This is the exact character of the rotation that is observed in MRX.

IV. FLUX ROPE STABILITY CHARACTERISTICS

In order to quantitatively analyze the stability properties of these flux ropes, we examine magnetic fluctuations that are measured by the rake-shaped 90-channel magnetic probe. In particular, we choose signals from individual magnetic pickup coils that are located near the edge of the probe. These edge coils remain outside of the flux rope for the duration of the discharge and therefore measure only external magnetic fluctuations. A sample poloidal field fluctuation signal $\delta B_P(t)$ is plotted in black in each panel of Fig. 5. It is clear from these signals that the external magnetic fluctuations persist until a certain stabilization threshold is crossed where the plasma quickly ceases its kinking motion.

To identify this stabilization threshold, we focus on the transition from unstable to stable behavior that occurs between 400 and 600 μs. During this time, the flux rope equilibrium evolves rather slowly such that the stabilization time can be accurately determined. The stabilization time is measured by identifying the time where the kink oscillation amplitude drops below a few gauss without reappearing. This stabilization time will correspond to a single "threshold q_a" value (i.e., the q_a value at the transition to stability), which can be determined from experimentally-measured discharge parameters. In order to calculate the threshold q_a value, the various components of Eq. (2) must be collected for a given discharge. Here, we assume that the flux rope minor radius a

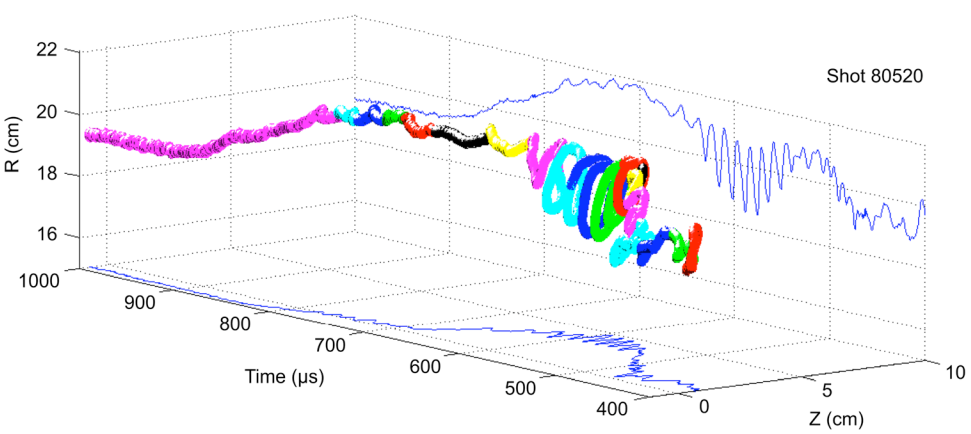

FIG. 4. (Color online) Time evolution of the *Z-R* flux rope center at one toroidal location between the electrodes in a discharge with $\Theta=90°$. For this analysis, the flux rope center is defined as the center-of-mass of the 2D current density profile that is measured by the 90-channel magnetic probe. The flux rope shown here is unstable early in the discharge as indicated by the coherent rotating motion in the *Z-R* plane. False color is added to better visualize the motion. The flux rope stablizes later in time after the plasma current begins to decline.

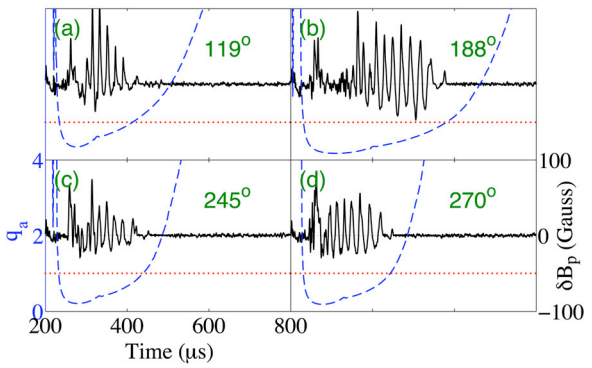

FIG. 5. (Color online) Time evolution of the q_a value (dashed blue lines, left axis) and magnetic fluctuation amplitude (solid black lines, right axis) for several flux ropes of varying electrode separation angle. The KS stability threshold ($q_a = 1$) is marked by the dotted red line in each subplot. The fluctuation traces are taken from one of the pickup coils in the 2D 90 channel probe array that is outside the edge of the plasma. The fluctuations that result from the external kinking and rotation of the plasma column stop when $q_a \simeq 1$.

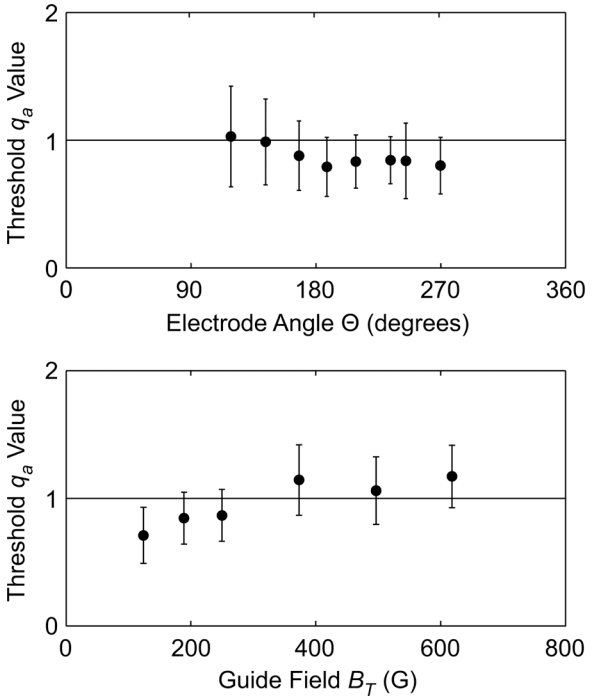

FIG. 6. (a) The measured threshold q_a value as a function of the electrode separation angle Θ. Here $B_T = 120$ G and $a = 7.3$ cm. The black solid line marks the $q_a = 1$ Kruskal-Shafranov limit. (b) The measured threshold q_a value as a function of guide field strength B_T. Here the electrode angle is $\Theta = 270°$ and again $a = 7.3$ cm. The error bars are calculated by combining the uncertainty in the individual threshold q_a measurements with the statistical variation over multiple shots.

is set by the cathode minor radius and that the toroidal field B_T is given by the guide field strength at the center of the electrodes. These assumptions are supported by fast camera images that show that a varies little from cathode to anode and that the flux rope expands only slightly such that B_T is relatively constant. The plasma current waveform $I_p(t)$ is measured using a current transformer and the flux rope length waveform $L(t)$ is measured by the various toroidally-distributed magnetic probes (as described in Sec. II). The calculated q_a evolution is plotted in Fig. 5 (dashed blue lines) for each of the four sample discharges, which have different electrode separation angles. The separation angle Θ is scanned in order to modify the flux rope length because $L \sim \Theta$. Due to the different flux rope lengths, the plasma stabilizes at a different time in each case. Note, however, that this time is always near $q_a \simeq 1$. In many cases, the stabilization time can also be verified by observing changes in the fast camera images.

We can now rigorously test the applicability of the Kruskal-Shafranov limit introduced earlier in this paper to the partial-toroidal flux ropes produced in MRX. This is done by independently scanning the various quantities that modify the edge safety factor q_a. Since the plasma current I_p is already scanned within each discharge by the rise and fall of the current waveform, we focus here on scans of the electrode separation angle Θ (which changes the flux rope length L) and of the toroidal (guide) field B_T. The collection of threshold q_a values obtained from these parameter scans is shown in the two panels of Fig. 6. It is clear that in both cases the stabilization threshold remains close to $q_a = 1$ throughout the scans. This serves to verify that the KS theory captures the key physics of stability in these partial-toroidal flux ropes.

As mentioned in the introduction, if the flux rope were instead free to move at one end, then the stabilization threshold is predicted to change to $q_a = 2$. This behavior is clearly not observed here. It is also worth noting that if both ends of the flux rope were free to move, the stabilization threshold would also be $q_a = 1$. We are able to rule out this possibility, however, by examining the envelope of the kink oscillations in these flux ropes. The toroidally-distributed array of 1D magnetic probes measures the displacement of the flux rope as a result of its kinking motion. We observe that the displacement amplitude is at its largest near the midpoint between the electrodes and at its smallest at the electrodes, especially the cathode. Thus we conclude that these partial-toroidal plasmas obey the $q_a = 1$ Kruskal-Shafranov limit for non-periodic flux ropes with two fixed boundaries.

V. SUMMARY AND DISCUSSION

In summary, the stability characteristics of partial-toroidal flux ropes formed between two electrodes of the same size have been examined in the laboratory. Magnetics measurements clearly show that the external kink stability threshold for these plasmas is governed by the Kruskal-Shafranov limit for a flux rope with two fixed boundaries ($q_a = 1$). This behavior is verified across a wide range of discharge parameters using scans of the applied toroidal field, the plasma length, and the plasma current. Despite several pre-existing experimental studies of flux rope stability, this work represents the first definitive identification of $q_a = 1$ stability in laboratory flux ropes with two fixed boundaries.

As outlined in the introduction, the difficulty in experimentally identifying $q_a = 1$ stability behavior is largely due to the uncertainty and variability of the boundary condition at the anode. This can result, for example, from the formation of a resistive sheath near the anode surface or from the presence of a plasma/vacuum interface at the anode end of

the discharge. In the experiments presented here, we believe that the fixed-boundary behavior at the anode is a result of the direct matching of the anode minor radius to the minor radius of the flux rope, which is set by the cathode size. Thus, even if a resistive sheath forms as described in Refs. 23–25, the limited extent of the anode surface inhibits the motion of the end of the flux rope such that the anode appears as a second fixed boundary to the flux rope plasma. This direct matching condition does not exist in any of the prior linear flux rope experiments.[24–28]

The results presented here also represent the first experimental identification of $q_a = 1$ stability in a partial-toroidal system. Though this lack of dependence on toroidicity is not surprising given the success of the KS theory in explaining tokamak stability, it does reinforce the potential applicability of these results to other partial-toroidal systems. These include the many theoretical models of coronal eruptions that invoke partial-toroidal flux ropes whose footpoints are anchored (fixed) in the dense photosphere.[3,13,16]

There are several extensions of these partial-toroidal flux rope experiments that will be investigated in the near future. These include studying cases where the anode is much larger than the cathode in order to permit the plasma column to move freely at one end. As mentioned, the stability criteria is predicted to change to $q_a = 2$ for this case. Another area of interest concerns the evolution and force balance of the equilibria observed in these experiments. The equilibrium reconstructions used in this paper for stability analysis are being further developed for use in comprehensive studies of these partial-toroidal equilibria. It is interesting to note that the flux ropes studied here evidently do not remain kink-stable via the equilibrium expansion mechanism suggested in Ref. 17. Thus, studying the equilibrium properties of these discharges may also provide additional understanding of the processes that govern their stability.

ACKNOWLEDGMENTS

The authors would like to thank R. Cutler for technical contributions. This work is supported in part by Contract No. DE-AC02-09CH11466 with the U.S. Department of Energy.

[1]*Coronal Mass Ejections*, edited by N. Crooker, J. A. Joselyn, and J. Feynman (American Geophysical Union Monograph, Washington, DC, 1997),
[2]R. Illing and A. Hundhausen, J. Geophys. Res. **90**, 10951, doi:10.1029/JA091iA10p10951 (1986).
[3]J. Chen, J. Geophys. Res. **101**, 27499, doi:10.1029/96JA02644 (1996).
[4]L. Burlaga, E. Sittler, F. Mariani, and R. Schwenn, J. Geophys. Res. **86**, 6673, doi:10.1029/JA086iA08p06673 (1981).
[5]Z. Mikić and J. A. Linker, Astrophys. J. **430**, 898 (1994).
[6]S. K. Antiochos, C. R. DeVore, and J. A. Klimchuk, Astrophys. J. **510**, 485 (1999).
[7]B. C. Low, Sol. Phys. **167**, 217 (1996).
[8]L. F. Burlaga, J. Geophys. Res. **93**, 7217, doi:10.1029/JA093iA07p07217 (1988).
[9]T. Amari, J. F. Luciani, Z. Mikic, and J. Linker, Astrophys. J. **529**, L49 (2000).
[10]X. Cheng, J. Zhang, Y. Liu, and M. D. Ding, Astrophys. J. Lett. **732**, L25 (2011).
[11]A. W. Hood and E. R. Priest, Sol. Phys. **64**, 303 (1979).
[12]D. M. Rust and A. Kumar, Astrophys. J. **464**, L199 (1996).
[13]P. A. Isenberg and T. G. Forbes, Astrophys. J. **670**, 1453 (2007).
[14]E. G. Zaidman and T. Tajima, Astrophys. J. **338**, 1139 (1989).
[15]T. G. Forbes, J. Geophys. Res. **95**, 11919, doi:10.1029/JA095iA08p11919 (1990).
[16]T. Török and B. Kliem, Astrophys. J. **630**, L97 (2005).
[17]J. Chen, "Coronal mass ejections: cause and consequences a theoretical view," in *Coronal Mass Ejections*, edited by N. Crooker, J. A. Joselyn, and J. Feynman (American Geophysical Union Monograph, Washington, DC, 1997), Vol. 99.
[18]M. Kruskal and J. L. Tuck, Proc. R. Soc. London, Ser. A **245**, 222 (1958).
[19]V. Shafranov, At. Energy **5**, 38 (1956).
[20]J. Wesson, *Tokamaks* (Clarendon, Oxford, 1987).
[21]I. M. Lanskii and A. I. Shchetnikov, Sov. J. Plasma Phys. **16**, 322 (1990).
[22]C. C. Hegna, Phys. Plasmas **11**, 4230 (2004).
[23]D. D. Ryutov, I. Furno, T. P. Intrator, S. Abbate, and T. Madziwa-Nussinov, Phys. Plasmas **13**, 2105 (2006).
[24]I. Furno, T. P. Intrator, D. D. Ryutov, S. Abbate, T. Madziwa-Nussinov, A. Light, L. Dorf, and G. Lapenta, Phys. Rev. Lett. **97**, 015002 (2006).
[25]X. Sun, T. P. Intrator, L. Dorf, I. Furno, and G. Lapenta, Phys. Rev. Lett. **100**, 205004 (2008).
[26]S. C. Hsu and P. M. Bellan, Phys. Rev. Lett. **90**, 215002 (2003).
[27]M. Zuin, R. Cavazzana, E. Martines, G. Serianni, V. Antoni, M. Bagatin, M. Andrenucci, F. Paganucci, and P. Rossetti, Phys. Rev. Lett. **92**, 225003 (2004).
[28]W. F. Bergerson, C. B. Forest, G. Fiksel, D. A. Hannum, R. Kendrick, J. S. Sarff, and S. Stambler, Phys. Rev. Lett. **96**, 015004 (2006).
[29]J. F. Hansen and P. M. Bellan, Astrophys. J. **563**, L183 (2001).
[30]H. Soltwisch, P. Kempkes, F. Mackel, H. Stein, J. Tenfelde, L. Arnold, J. Dreher, and R. Grauer, Plasma Phys. Controlled Fusion **52**, 124030 (2010).
[31]S. K. P. Tripathi and W. Gekelman, Phys. Rev. Lett. **105**, 075005 (2010).
[32]M. Yamada, H. Ji, S. Hsu, T. Carter, R. Kulsrud, N. Bretz, F. Jobes, Y. Ono, and F. Perkins, Phys. Plasmas **4**, 1936 (1997).